J Mater Sci (2007) 42:1847–1855
DOI 10.1007/s10853-006-0737-9

Nanostructured Al_2O_3–ZrO_2 composite synthesized by sol–gel technique: powder processing and microstructure

Debasish Sarkar · Deepak Mohapatra · Sambarta Ray · Santanu Bhattacharyya · Sukumar Adak · Niren Mitra

Received: 17 March 2006 / Accepted: 28 July 2006 / Published online: 9 January 2007

Abstract Al_2O_3–ZrO_2 composite gel powder was prepared by sol–gel route. The gel precursor compositions were preferred to achieve yield of 5–15 mol% zirconia after calcination of respective powders. The precursor gel was characterized by Differential Thermal Analysis (DTA)/Thermo Gravimetric (TG), IR and X-ray Diffraction study (XRD). The analysis reveal the gel contained pseudoboehmite and amorphous $Zr(OH)_4$, which was decomposed in three and two stages respectively. The phase transformation of alumina during calcination followed the sequence of pseudoboehmite $\rightarrow$ bayerite $\rightarrow$ boehmite $\rightarrow$ γ-Al_2O_3 $\rightarrow$ θ-Al_2O_3 $\rightarrow$ α-Al_2O_3, while that of ZrO_2 follows amorphous ZrO_2 $\rightarrow$ t-ZrO_2 $\rightarrow$ (t + m) ZrO_2. Fourier Transform Infrared Spectroscopy (FTIR) studies showed that the number of M–OH and M–O bond increases with zirconia due to a change in the cationic charge of the composite powder. Transmission Electron Microscopy (TEM) photograph of calcined powder exhibited the presence of dispersed as well as agglomerated nano sized spherical particles. SEM and Electron Probe Microscope Analysis (EPMA) confirmed the near uniform distribution of zirconia particles in the alumina matrix.

D. Sarkar (✉) · D. Mohapatra · S. Ray · S. Bhattacharyya · S. Adak
Department of Ceramic Engineering, National Institute of Technology, Rourkela 769008, Orissa, India
e-mail: dsarkar@nitrkl.ac.in

N. Mitra
Department of Chemical Technology, University of Calcutta, 92, APC Road, Kolkata 700009, West Bengal, India

Introduction

Alumina is an important structural ceramics having wide application potential. However, its use in real life systems is limited due to its low fracture toughness resulting in catastrophic failure. Among the several measures that are being taken to overcome the drawback, the addition of zirconia (platelet, particle, fiber) in the alumina matrix remarkably improves the toughness on account of stress induced transformation toughening [1, 2]. An excellent review by Basu has discussed the intricacies of transformation toughening mechanism and the factors affecting the toughening behavior of ZrO_2 based system [3]. It is well known that the extent of stress induced transformation toughening depends on the uniformity of dispersion of tetragonal ZrO_2 in alumina matrix, its volume fraction and transformability [4, 5]. The uniform dispersion of zirconia particles in the alumina matrix can be controlled by homogeneous powder synthesis techniques. A series of powder processing techniques have been used to synthesize homogenous powder mixture and amongst them the precipitation and the sol–gel methods are the easy and commercialized chemical synthesis routes for producing zirconia doped nanoparticles [6–10]. This method while providing a homogeneous and molecular level mixing of the precursors also ensures control of particle spacing and thus provides a uniform composite microstructure. Moreover, the crystallization of amorphous precursor to oxide powder is also obtained at a lower temperature than that observed for the powders prepared by conventional route. As a result the particle size of the individual oxides is the lowest in this process, which promotes enhanced densification at a lower temperature. A finer

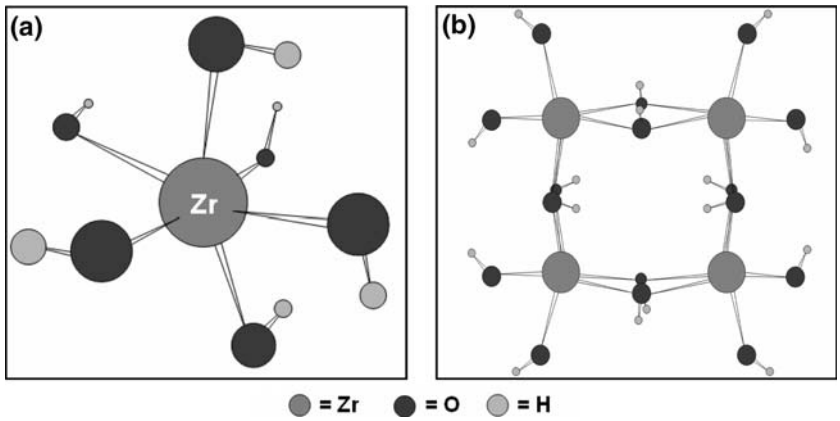

Fig. 1 Cluster structure of $[Zr(OH)_6]^{2-}$ (**a**), ordered structure of polymerization precursors (**b**) [14]

initial particle size of zirconia particles also produces a smaller final grain size in the sintered samples which further helps to retain the zirconia in tetragonal form.

Recently, Caracoche et al. synthesized nano-zirconia powders using the sol–gel method through pH control of the precursor solution [11]. Chen et al. also observed that in the pH range 7–10.5, the predominant monomer cluster is $[Zr(OH)_6]^{2-}$ (Fig. 1a), which preferentially produces tetragonal (t) precursor structure with slow alkali addition (Fig. 1b) [12]. Therefore, the bonding mechanisms of Zr–OH and its final phase content depends on bridging hydroxyl groups, monomer structure, polymerization kinetics and pH of the precursor solution.

The synthesis of ZrO_2 dispersed Al_2O_3 precursor powders from multiphase hydrogel is a complex subject, which depends on the configuration of hydroxide of Al and Zr and its polymerization. The chemistry and polymerization of aluminum oxide and hydroxide depend on acid/base properties. The proton activity is significantly affected by the oxygen coordination surrounding Al^{3+}. In the deprotonated form of the aluminum hydroxide in water $[Al(OH)_4]^-$, Al atom is tetrahedrally coordinated with oxygen atoms, whereas all the protonated cationic species in the series $Al(OH)^{2+}(aq)$ to $Al^{3+}(aq)$ are six-coordinated. This amphoteric nature of $Al(OH)_3$ in water is the cause for the stability of hydrogel [13]. Zakharchenya and Vasilevskaya investigated the influence of temperature on the dehydration and crystallization behavior of such stable hydrogel products [14].

The above discussion summarizes that the phase evolution sequence during crystallization of alumina–zirconia from its hydrated precursor depend among other factors on the nature and type of bonding present in the hydroxides of Al and Zr. Thus the decomposition behavior phase evaluation sequence and the nature of bond type on the phase evaluation of both Al and Zr hydroxide are studied by thermal analysis, X-ray Diffraction study (XRD) and Fourier Transform Infrared Spectroscopy (FTIR) in the as-prepared precursor as well as in the calcined powder . The effectiveness of the sol–gel process in achieving a uniform dispersion of alumina and zirconia in the calcined powder as well as sintered pellets is studied by Transmission Electron Microscopy (TEM) and SEM/Electron Probe Microscope Analysis (EPMA) combination.

Experimental

Aluminum nitrate (E-Merck, India) and zirconium oxychloride (E-Merck, India) were used as precursor for preparing high alumina–zirconia composite powder. Solutions of aluminium nitrate (0.5 M) and zirconium oxychloride (0.5 M) were mixed together in the required proportions to yield different Al_2O_3–$x$$ZrO_2$ (where x = 5, 7.5, 10 and 15 mol%) batches. The mixed hydrogel was obtained by drop wise addition of 1:1 NH_3 hydroxide solution into the continuously stirred mixed aqueous solution of Al and Zr salt maintained at 25 °C. The viscosity of the batch gradually increased and finally set to an enblock gel at pH ~ 9. The gels were then aged at room temperature for 48 h. Subsequently, the gel of each composition was washed repeatedly with boiling distilled water to remove chloride and nitrate ions and filtered. The filter cake was oven dried. The dried gels were calcined in air in a muffle furnace at different temperatures varying from 200 °C to 1400 °C with a hold time of 2 h at the corresponding peak temperatures. The composition of each batch has been listed in Table 1.

For phase analysis, XRD of the dried gel and calcined powders were carried out in a Philips X-ray diffractometer (PHILIPS PW1830), using Cu-Kα

Table 1 Composition of the gel precursor

Identification	Al_2O_3 (mol%)	ZrO_2 (mol%)
A5Z	95	5
A75Z	92.5	7.5
A10Z	90	10
A15Z	85	15

radiation. The voltage and current setting were 35 kV and 30 mA respectively. The samples were continuously scanned with a step size of 0.02^0 (2θ) and a count time of 1 s per step. Silicon was used as an internal standard. The crystallite size of the synthesized powder was determined from X-ray line broadening using the Scherrer's equation as follows:

$$D = \frac{0.9\ \lambda}{B \cos \theta} \quad (1)$$

where D is the crystallite size (nm), λ is the wavelength of the X-ray radiation (1.54056 Å), θ is the Bragg's angle and B is the full width at half maximum (FWHM), where $B = (B^2_{\text{meas}} - B^2_{\text{Equip}})^{1/2}$. B_{meas} = Measured FWHM and B_{equip} = FWHM due to instrumental broadening.

The thermal decomposition behavior of the washed and dried gel was studied by Thermo Gravimetric (TG) – Differential Thermal Analysis (DTA) analysis (Netzsch STA 409C) upto 1200 °C at a heating rate of 10 °C/min. TEM was used to estimate the particle size and morphology of the powder and observe the morphology and agglomeration state of A15Z powder. TEM observations were carried out at 120 kV (Model JEM-2000 FX, JEOL, Japan) having a point-to-point resolution of 5 Å. For TEM observations, powders were dispersed in ethyl alcohol using an ultrasonic treatment and a microdrop of the resulting suspension was placed on carbon-coated copper grids. The particle dimensions were measured from TEM micrographs. At least 400 particles were measured to reach an average particle size value. The particle size distribution (volume percent) of the calcined powder was carried out using laser particle size analyzer (Malvern, Mastersizer 2000, UK). Surface area of the as-dried gel powder was carried out by nitrogen adsorption using BET surface area analyzer (Quantachrome, USA). FTIR analysis of dried gel and calcined powders were carried out in a DRIFT Magna IR560, Nicolet spectrometer in the wavenumber range 400–4000 cm^{-1} at resolution of 4 cm^{-1} for studying the chemical groups on the surface of the as-dried gel as well as calcined powder. A small amount of sample (0.2 gm) was thoroughly mixed with ground KBr in an agate mortar and a disc was prepared in vacuum maintaining a pressure of 33 kg/cm^2. The precursor was calcined at 1000 °C for 2 h, uniaxially pressed at 250 MPa with addition of 5 weight percent uncalcined gel-precursors as binder, followed by cold isostatic press at 300 MPa and green compacts were sintered at 1550 °C for 4 h. The thermally etched (1500 °C for 30 min) and mounted samples were sputter coated with palladium–gold under vacuum of 0.01 Torr for preventing surface charging. The coated specimens were studied by SEM (JEOL-JSM840) with an EPMA attachment.

Results and discussions

FTIR analysis

The major peaks appearing in the FTIR spectra of alumina–zirconia hydroxide system could be related to the following:

(1) –OH stretching vibration of the surface bonded or adsorbed water
(2) –OH bending vibration of the surface bonded or adsorbed water
(3) –OH stretching vibration of structural water, corresponding to M–OH bonding
(4) –OH bending vibration of structural water, corresponding to M–OH bonding
(5) Al–O stretching vibration
(6) Zr–O stretching vibration

The IR spectral frequency of uncalcined hydrogels and calcined powders of all the compositions are presented in Table 2 and the detailed IR spectra of the A15Z powder calcined at different temperatures have been shown in Fig. 2. All the gels and calcined samples exhibited –OH *stretching vibration* in the frequency range of 3136–3857 cm^{-1}. The reduced reflectance and bond depth of the gel powder could be ascribed to the noncrystalline nature of the material [13]. The number of peaks for –OH stretching vibration in the Al_2O_3–ZrO_2 powder increases with an increase in the ZrO_2 content. The increased IR interaction probably reflects a gradual change in the composition and heterogeneity in the bond as well as a switchover from a homogenous single phase structure to a homogenous two phase structure.

The frequency of different vibrational modes of Al–OH and/or Zr–OH including the bending and stretching modes are altered due to change in the charge distribution among molecules. This altered frequency of vibration in turn causes a change in the electrical dipole moment of the original species. The charge distribution around each Al–OH and/or Zr–OH and

Table 2 IR spectral frequency (cm^{-1}) of Al_2O_3–ZrO_2 systems with respect to temperatures

Material	Dried gel	200 °C	400 °C	1000 °C
A5Z	3656.2	3657.1	3461	3484.3
	3553.3	3620.7		
	3471.8	3553.2		
	3146.2	3466.9		
		3141.6		
	2365.7	2396.1	2371.4	
	2089.9	2065.6		1643.7
	1762.0	1762.7	1636.6	1395.9
	1629.7	1632.6	1384.7	
	1383.9	1384.8		
	1070.8	1025.6		
	978.7	978.2		839.8
	767.7	765.9	596.7	537.4
	515.8	526.9		
	3656.3		3449.2	3484.3
	3553.3			
	3468.9			
	3140.8			
	2396.8		2368.1	
A75Z	2065.5			
	1763.0		1637.8	1642.3
	1630.9		1385.5	1425.3
	1387.3			
	978.7			846.2
	767.0		582.2	542.3
	523.2			
	3656.5	3465.5		3484.3
	3552.3	3144.0		
	3472.5			
	3139.3			
	2396.2	2369.0		
A10Z	2065.7			
	1763.0	1629.6		1641.2
	1631.8	1380.6		
	1385.2			
	1070.4	1065.5		832.8
	977.0			
	760.5	767.9		568.0
	514.3	523.8		
	3857.5	3447.9	3449.9	3450.8
	3656.4			
	3552.0			
	3471.5			
	3425.8			
	3136.0			
	2396.6	2361.7	2371.8	
A15Z	2066.3			
	1763.1	1638.2	1636.2	1629.5
	1634.8	1385.3	1385.4	
	1385.0			
	1069.6	667.9		828.0
	977.1			
	825.3			
	762.8		585.3	525.6
	515.6			

associated vibration is influenced by the charge on its neighboring species. Hence, the continuum vibration of the matrix is responsible for the change in dipole moment and establishment of an electric field of the composite powder. The increased cationic charge in the alumina–zirconia composite powder due to the introduction of Zr^{4+} interacts strongly with the polar inner hydroxyl groups. This interaction probably results in the reduction of vibrational dipole moment in bending thereby creating a greater force of attraction (antisymmetric coupling) on the stretching vibration.

The stretching vibration for structural –OH and adsorbed water appear at wave number greater than 3000 cm^{-1} for all the AZ compositions. A careful inspection of stretching frequencies reveal that an increase in ZrO_2 content in the batch causes a significant change in the –OH stretching pattern upto 10% ZrO_2 addition for A5Z to A10Z samples. Four peaks are observed in the wave number range 3656, 3553, 3471 and 3146 cm^{-1} which account for –OH stretching. In the A15Z samples two more additional peaks appear at 3857 and 3425 cm^{-1} (Fig. 2a), which indicate the presence of more –OH in this batch. These two additional vibrations are probably due to –OH groups attached to the Zr^{+4}.

For all AZ samples the vibrations appearing in the range 2396–2065 cm^{-1} could be assigned to the coupling effect of *stretching and bending vibrations* of –OH groups. The peaks which appear at 1764, 1634 and 1385 cm^{-1} are due to the *bending vibration* of Zr–OH groups. The peak positions are more or less the same in all the samples. The peaks between 1070 and 760 cm^{-1} correspond to *Al–O vibration* [15]. The strong absorption band of the latter one may be attributed to six-coordinated Al^{3+} ions. These O–H and Al–O vibrations are characteristics of pseudoboehmite. The absorption band at 1070 cm^{-1} is due to the presence of alumina gel. The above results conclude that alumina in this particular alumina–zirconia system is present as an intermediate bayerite. The –OH stretching and bending vibrations is exhibited by both the constituents of the hydrogels. The absorption bands at 514–523 cm^{-1} correspond to *Zr–O vibrations*.

A5Z samples calcined at 200 °C shows an additional peak at 3620.7 cm^{-1}. This is related to the activation of the structure by heating and consequent adsorption of water to the active surface. The bending vibration at 1762.7 cm^{-1} shows an additional peak due to adsorbed water. The IR analysis of A10Z and A15Z samples shows the disappearance of peaks at 3656 cm^{-1} (due to the stretching vibration of physically adsorbed –OH with Al^{+3}) and 3552 cm^{-1} (due to the stretching vibration of physically adsorbed –OH with Zr^{+4}) after calcination at 200 °C. The disappearance of peaks corresponding to adsorbed water in A15Z sample

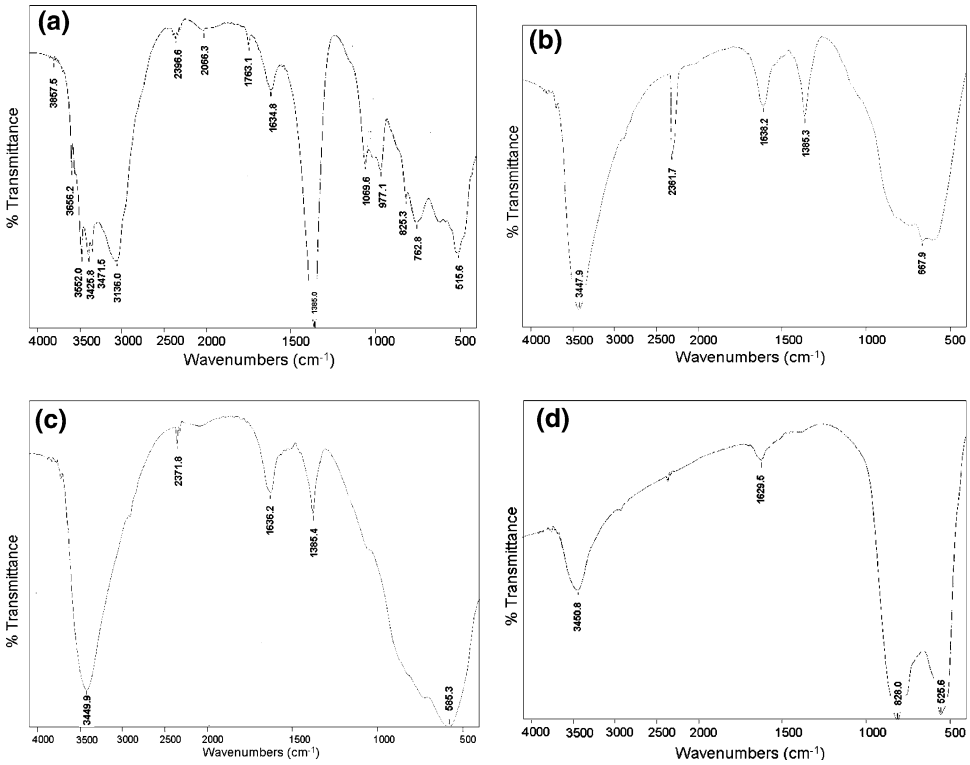

Fig. 2 Fourier Transform Infrared Spectroscopy (FTIR) curves of Al_2O_3–15ZrO_2 (mol%) (**a**) dried gel (**b**) 200 °C (**c**) 400 °C (**d**) 1000 °C

could be related to the reduction in surface positive charge density of Al_2O_3–ZrO_2 system with the increase in ZrO_2 content. The –OH group bonded with Al^{+3} shows a peak at 3447.9 cm^{-1} with the corresponding bending vibrations at 1638.2 and 1385.3 cm^{-1} (Fig. 2b). Bending vibration and/or coupled vibration of –OH group attached with Zr^{+4} disappeared at this temperature.

After calcination at 400 °C, for A5Z batch, all the peaks related to stretching vibration of free and bonded water disappear. Only one peak at 3461 cm^{-1} still exists, which is related to the stretching vibration of –OH group attached with Al^{+3}. Bending vibration and/or coupled vibration of Al–OH group can only be observed in the spectrogram. On the lower frequency side a peak at 596.7 cm^{-1} is observed which could be related to the Al–O vibration. Heating at 400 °C causes broadening of peaks in the lower frequency range (500–1000 cm^{-1}) due to overlapping of Al–O and Zr–O infrared vibrations of transition alumina and zirconia phases. Thus individual peaks corresponding to Zr–O could not be detected in the temperature range 200–400 °C. However, at higher temperature (1000 °C) peaks corresponding to Al–O and Zr–O could be clearly observed. Similar trend is also followed in A75Z, A10Z and A15Z samples.

IR spectra shows that a trace amount of –OH group still remains in the structure of ZrO_2 dispersed Al_2O_3 powder even after heating at 1000 °C. The reduced intensity of –OH absorption band could be due to the moisture absorption during testing. A10Z powder calcined at 1000 °C shows a peak at 3484.3 cm^{-1} corresponding to Al–OH stretching vibration. The stretching of crystalline Al–O and Zr–O bonds show absorption bands at lower frequencies of 828.0 cm^{-1} and 525.6 cm^{-1} respectively for A15Z samples [16].

XRD analysis

The sequence of phase evaluation in the calcined A15Z hydrogel was studied by XRD. The XRD pattern of the as dried gel (Fig. 3) shows broad peak of bayerite only. The broad peak of bayerite indicates the presence of fine crystallites (crystallite size 5–20 nm). XRD of hydrogel calcined at 200 °C have both bayerite ($Al(OH)_3$) and boehmite (Al(O)OH). Boehmite crystallizes from bayerite on heating according to the reaction:

$$Al(OH)_3 = Al(O)OH + H_2O \quad (2)$$

The IR analysis of hydrogel also confirms the presence of intermediate boehmite as well as Zr–O bond of noncrystalline zirconia (Fig. 2a). Calcination at higher temperature (1000 °C) induces further phase transition in boehmite as well as crystallization of zirconia from amorphous zirconium hydroxide (Fig. 3b). At this

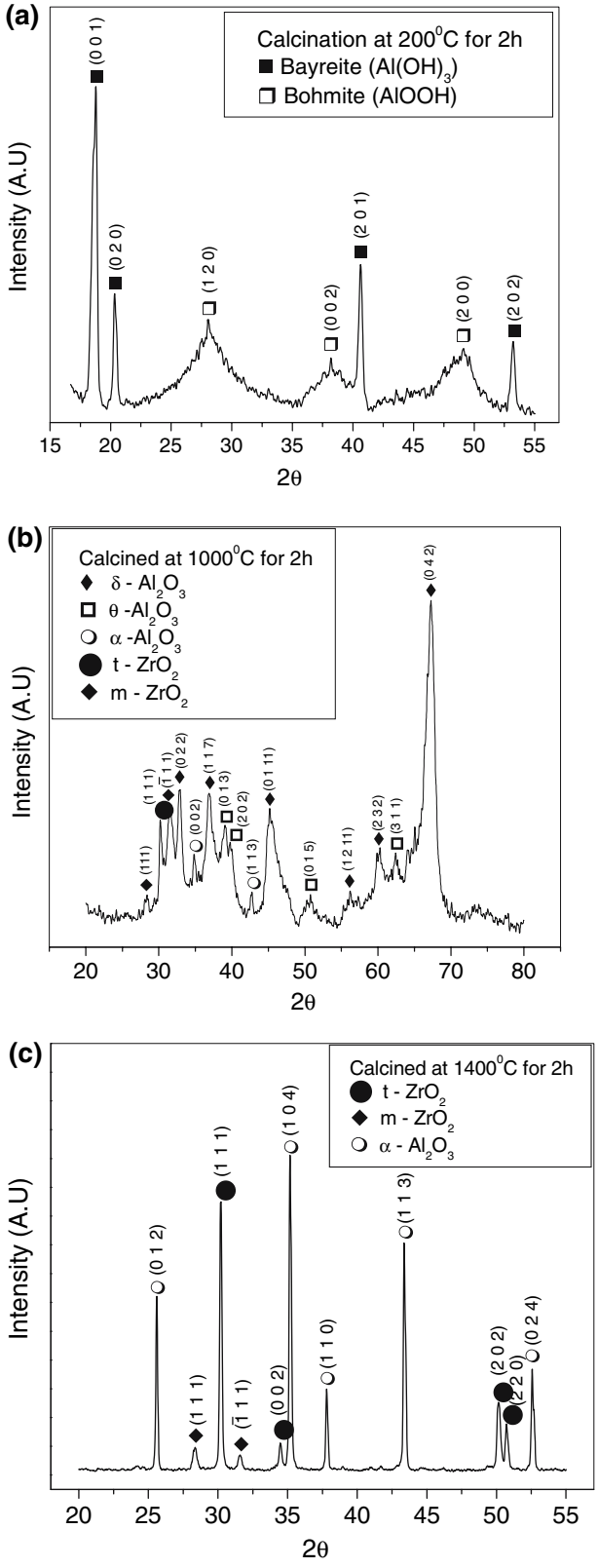

Fig. 3 Phase analysis of Al_2O_3–15ZrO_2 (mol%) powders calcined at (**a**) 200 °C for 2 h (**b**) 1000 °C for 2 h and (**c**) 1400 °C for 2 h

temperature, the following phases were identified m-ZrO_2, t-ZrO_2, δ-Al_2O_3, θ-Al_2O_3 and α-Al_2O_3. The crystallite size of the calcined powder at 1000 °C for 2 h is in the range of 20–160 nm. Usually α-Al_2O_3 crystallizes around 1200 °C, however, in the present study the lower crystallization temperature of α-Al_2O_3 could be related to the fine crystallite size and higher specific surface area. The phases present at the highest treatment temperature (1400 °C) are α-Al_2O_3, t-ZrO_2 and m-ZrO_2 (Fig. 3c). A series of XRD phase investigation or crystallization behavior of the A15Z gel precursor is listed in Table 3. The careful observation of the above data, it is emphasizing that phase transformation route from pseudoboehmite to α-Al_2O_3 is deviating from earlier researcher's works [17], this is presumably due to the difference in particle size and content of external zirconia phase. The increase in m-ZrO_2 content at 1400 °C results from an increase in the grain size of zirconia, which induces partial t–m transformation during cooling. Thus XRD analysis of A15Z emphasizes that the phase transformation from bayerite to α-Al_2O_3 agrees well with earlier studies [18]. The reduction of specific volume to the extent of 24% is observed during phase transformation of boehmite (0.332 cc/g) to α-Al_2O_3 (0.251 cc/g), probably results in the generation of intraparticle porosity in the alumina particles [19].

Thermal behavior of hydrogel

The DTA-TG curve of the dried A15Z gel powder is shown in Fig. 4. In the temperature range 50–300 °C DTA curve shows a broad endothermic peak at 110 °C, a sharp exothermic peak at about 225 °C

Table 3 Phase analysis of A15Z at different temperature by X-ray Diffraction (XRD) technique

Drying/calcinations temperature of gel	Phase content
70 °C	SB
200 °C	BH, B
400 °C	GA
600 °C	GA
800 °C	TZ, GA
900 °C	TZ, DA, TA, AA
1000 °C	MZ, TZ, DA, TA, AA
1100 °C	MZ, TZ, DA, TA, AA
1200 °C	MZ, TZ, DA, TA, AA
1300 °C	MZ, TZ, AA
1400 °C	MZ, TZ, AA

AA = α-Al_2O_3, B = Bayerite, BH = Bohemite, DA = δ-Al_2O_3, GA = γ-Al_2O_3, MZ = Monoclinic ZrO_2, SB = Pseudo Bohemite, TA = θ-Al_2O_3, TZ = Tetragonal ZrO_2

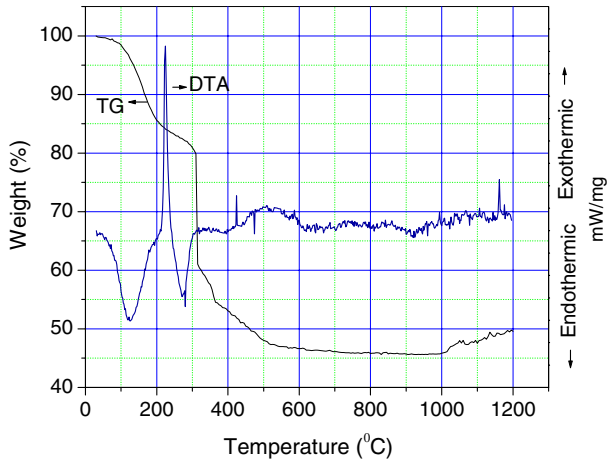

Fig. 4 Thermo Gravimetric (TG)/Differential Thermal Analysis (DTA) plot for the Al_2O_3–$15ZrO_2$ (mol%) precursor powders in air

and another endothermic peak at 280 °C. At higher temperature, the DTA curve shows a sharp and a small exothermic peak at about 420 °C, a sharp but small endothermic peak at about 480 °C. Finally, the DTA curve shows a small exothermic peak at about 1160 °C. The TG curve of the gel shows a gradual weight loss of about 15% in the temperature range 25–210 °C and a sharp weight loss of about 18% in the temperature range 210–315 °C show a further weight loss of about 17% which takes place in three stages. The first stage of this weight loss is about 5% in the temperature range 315–320 °C, the second stage about 10% in the temperature range 320–455 °C and the final stage of weight loss is about 2.0% in the temperature range 455–545 °C.

The above thermal behavior of the A15Z gel powder could be explained according to following: The gel powder contains disordered pseudoboehmite at room temperature having more than 15% excess water in its lattice [20]. The theoretical weight loss due to dehydroxylation of pseudoboehmite is about 13% for A15Z sample which matches well with the observed weight loss. Thus the first endothermic peak and the associated weight loss correspond to the dehydroxylation of pseudoboehmite. The dehydroxylation of pseudoboehmite is associated with the crystallization of bayerite (β-$Al_2O_3 \cdot 3H_2O$). Thus the exothermic peak could be related to the crystallization of bayerite. The bayerite thus formed undergoes further dehydroxylation to boehmite (α-AlOOH) in the temperature range 280–308 °C. The theoretical weight loss for this reaction is 19.61%. The observed weight loss 19% agrees well with this transformation. Subsequently, boehmite changes to γ-Al_2O_3 according to the reaction,

$$2AlO(OH) = Al_2O_3 + H_2O \quad (3)$$

The theoretical weight loss is 15% and for A15Z this will be 12.75%. The observed weight loss agrees well with the theoretical loss. The weight loss is associated with one exothermic and one endothermic peak. The presence of these peaks could be explained as follows: AlO(OH) does not transform to γ-Al_2O_3 directly. Literature reviewed says that AlO(OH) first transforms to an amorphous alumina on dehydroxylation which subsequently crystallizes to γ-Al_2O_3 [21]. Thus the exothermic and endothermic peaks in the temperature range 415–480 °C corresponds to the conversion of dehydroxylated boehmite to γ-Al_2O_3 via the intermediate step of amorphous alumina. Finally the exothermic peak at 1160 °C corresponds to crystallization of α-Al_2O_3. However, X-ray diffractograms of powders calcined for 2 h at 1000 °C show the presence of α-Al_2O_3. The difference in crystallization temperature of α-Al_2O_3 as observed in DTA and XRD could be because of the difference in heating schedule for the two samples. While X-ray pattern was recorded on samples which were held for 2 h at 1000 °C, the DTA was done without any isothermal hold. Thus the isothermal hold at 1000 °C has accelerated the transformation to α-Al_2O_3 at lower temperature. Similar change in the crystallization temperature of α-Al_2O_3 was also observed by the same research group in an earlier work [22].

On the other hand, the transformation of $Zr(OH)_4$ to ZrO_2 follows the reaction [23]:

$$Zr(OH)_4 = ZrO_{1.5}(OH) + 1.5H_2O \quad (4)$$

$$ZrO_{1.5}(OH) = ZrO_2 + 0.5H_2O \quad (5)$$

The theoretical weight loss for the dehydroxylation of $Zr(OH)_4$ and its crystallization to ZrO_2 following the above reaction sequence of Eqs. 4 and 5 should be about 4%. The observed weight loss matches well with the theoretical value.

TEM analysis

The TEM micrographs (Fig. 5) show uniform distribution of fine sized particles (light shade) in the range (≤20 nm). Thus the prepared powder was in the nanometer range. The micrograph also show a number of dark patches (about 100–180 nm) which indicate the agglomerated particles cluster which probably have resulted during sample preparation. The particle size analysis (Fig. 6) of the calcined powder also shows that the particles have a bimodal size distribution. The finer

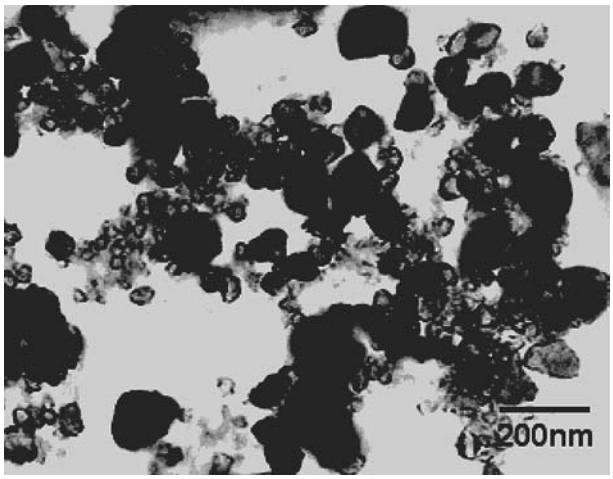

Fig. 5 Transmission Electron Microscopy (TEM) photograph of 15 mol% ZrO_2 doped Al_2O_3 powder. Precursor powder was calcined at 1000 °C for 2 h

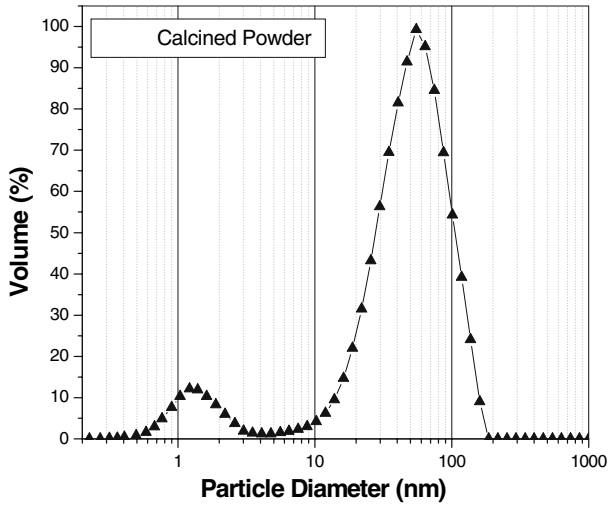

Fig. 6 Particle size analysis of calcined powder at 1000 °C for 2 h

particle (≤20 nm) represents the unagglomerated particles while the larger size particle (60–180 nm) represents the agglomerate size. The measured BET specific surface area of the calcined powder (1000 °C for 2 h) was found to be 130 m^2/g. The surface area data could be utilized to indirectly determine the particle size of the powder using the Eq. 6 [24] :

$$D = 6/\rho S \quad (6)$$

where D is the particle size, ρ is the theoretical density of the powder and S is the specific area.

Assuming the particles to be spherical in nature and the theoretical density of A15Z to be 4.28 gm/cc the calculated particle size was found to be ~10 nm. Thus

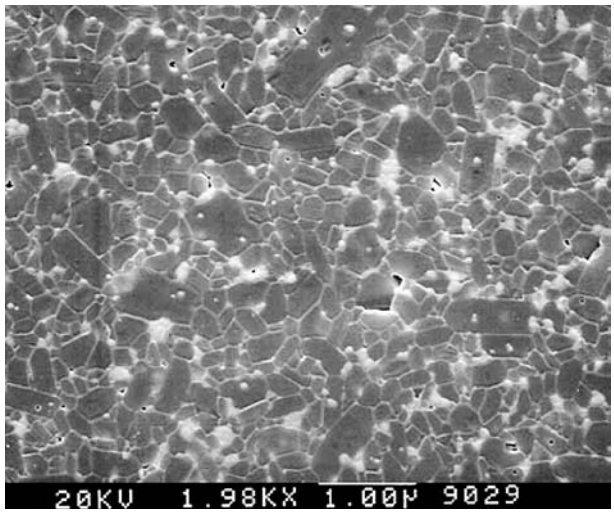

Fig. 7 Scanning back-scattered electron microscopy images showing the microstructure of polished and thermal etched surface Al_2O_3–15 mol% ZrO_2 (sintered at 1550 °C for 4 h). The phases with darker and white and contrast indicate Al_2O_3 and ZrO_2 respectively

the calculated particle size agrees well with the particle size measured from TEM photograph.

Scanning electron microscopic analysis

As shown in Fig. 7, the zirconia particles are in range of 30–240 nm, whereas the alumina grains are in the range 0.04–0.6 μm. The Al_2O_3 and ZrO_2 grains are dark and bright respectively. The ZrO_2 is usually at the triple point with two Al_2O_3 grains and show smaller dihedral angle than the Al_2O_3 grains. However, small fractions of intragranular zirconia grain are also noticed. The microstructure also contains tiny pores at isolated pockets. It can be seen that voids are nucleated mainly at grain boundary or at triple points and grow around the matrix grain. The fine cavities do not grow readily to the large ones because cavity growth is constrained by the surrounding matrix. Based on this, it is thought that in addition to diffusion, zirconia grains in alumina matrix act to mitigate localized stress concentrations and suppress cavity generation. However, the properties are governed by a combination of the behavior of the two grain sizes and morphology [25].

The X-ray mapping (EPMA analysis) of polished and thermally etched surface showing the presence of different elements (Al and Zr) within the matrix is illustrated in the Fig. 8. The Zr mapping (Fig 7b) shows an almost uniform distribution of ZrO_2 in the alumina matrix. However, considering the size and distribution of Zr X-ray mapping, it may be inferred

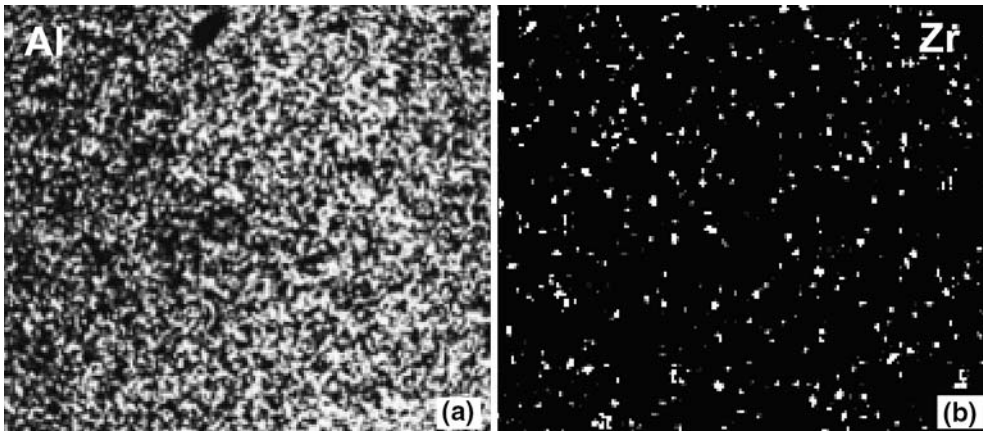

Fig. 8 X-ray mapping micrographs of different elements (**a**) Al and (**b**) Zr of sintered and polished surface

that some zirconia particles are in an agglomerated state, although the volume fraction of agglomerated zirconia is less. This homogeneous distribution assists to enhancement of the thermo-mechanical properties [26]. Thus it can be inferred that the distribution of zirconia in the sintered samples remain unaltered with increasing zirconia content. The near homogenous distribution of alumina and zirconia in the sintered samples of both A5Z as well as A15Z samples indicate that alumina and zirconia were uniformly distributed in the sintered samples as well as calcined powders of all the compositions studied. This homogenous distribution of alumina and zirconia is due to homogeneous particle size distribution of the starting powders.

Conclusions

The decomposition and crystallization of pseudoboehmite to γ-Al_2O_3 occurred in three stages. The transition from γ-Al_2O_3 to α-Al_2O_3 followed the intermediate stage of θ-Al_2O_3 formation. On the other hand, the crystallization of t-ZrO_2 from $Zr(OH)_4$ in single stage. The number and intensity of M–OH and M–O bonds increase on increasing ZrO_2 content. The sol–gel derived ~20–180 nm nanopowder became relatively coarser (ZrO_2 30–240 nm and Al_2O_3 0.04–0.6 μm) after sintering at 1550 °C. Particle size distribution indicates a bimodal size distribution with the highest particle size around 180 nm. Thus the size distribution indicates both unagglomerated and agglomerated particles.

References

1. Wefers K, Misra C (1987) Alcoa Technical Paper No. 19, Alcoa Laboratories, Pittsburgh, PA
2. Yarbrough WA, Roy R (1987) J Mater Res 2(4):494
3. Basu B (2005) Int Mater Rev 50(4):239
4. Basu B, Vleugels J, Van Der Biest O(2004) Mat Sci Engg A 366(2):338
5. Venkateswaran T, Sarkar D, Basu B (2005) J Am Ceram Soc 88(3):691
6. Hori S, Yoshimura M, Somiya S (1984) Am Ceram Soc. Columbus, OH, 794
7. Sproson DW, Messing GL (1984) J Am Ceram Soc 67(5):C92
8. Aksay IA, Lange FF, Davis BI (1983) J Am Ceram Soc 66(10):C190
9. Wu Y, Bandyopadhyay A, Bose S (2004) Mat Sci Engg A 380:349
10. Kagawa M, Kikuchi M, Syono YN (1983) J Am Ceram Soc 66(11):751
11. Caracoche MC, Rivas PC, Cervera MM, Caruso R, Benavádez E, De Sanctís O, Mintzer SR (2003) J Mater Res 18:208
12. Chen SG, Yin YS, Wang DP (2004) J Mol Struct 690:181
13. Guo GY, Chen YL (2001) J Mater Chem 11:1283
14. Zakharchenya RI, Vasilevskaya TN (1994) J Mater Sci 29:2806
15. Colomban PH (1989) J Mater Sci 24:3002
16. Low M, Mcpherson R (1989) J Mater Sci 24:892
17. Gitzen WH (1970) Am Ceram Soc Columbus, OH, 17
18. Lee HY, Werner R, Mordike BL (1992) J Eur Ceram Soc 10:245
19. Roger BB, Messing GL (1992) J Am Ceram Soc 82:825
20. Levin I, Brandon D (1998) J Am Ceram Soc 81(8):1995
21. Paglia G (2004) PhD Dissertation. Curtin Univeristy of Technology, Australia
22. Bhattacharyya S, Bharati S, Pratihar SK, Sinha RK, Behera RC, Ganguly RI (2003) Trans Indian Ceram Soc 62(1):18
23. Clearfield A, Nancollas GH, Blessing RH (1973) Ion exchange and solvent extraction. Marcel Dekker, New York, p 5
24. Rahaman MN (1995) Ceramic processing and sintering. Marcel Dekker, Inc, New York, p 115
25. Kim BN, Hiraga K, Morita K, Sakka Y (2001) Acta Mater 49:887
26. Sarkar D, Adak S, Cho SJ, Chu MC, Mitra NK (2007) Ceram Inter 33(2):255